

Anisotropic two-dimensional magnetoexciton with exact center-of-mass separation

Dang-Khoa D. Le,¹ Hoang-Viet Le,¹ Dai-Nam Le,² Duy-Anh P. Nguyen,³
Thanh-Son Nguyen,⁴ Ngoc-Tram D. Hoang,¹ and Van-Hoang Le¹

¹*Computational Physics Key Laboratory K002, Department of Physics,
Ho Chi Minh City University of Education, Ho Chi Minh City 72759, Vietnam*

²*Department of Physics, University of South Florida, Tampa, Florida 33620, USA*

³*Thu Dau Mot University, Phu Loi, Ho Chi Minh City 75110, Vietnam*

⁴*Faculty of Fundamental Sciences, University of Architecture Ho Chi Minh City, Ho Chi Minh City 722700, Vietnam*

(Dated: March 3, 2026)

Excitons in anisotropic two-dimensional (2D) materials, defined by direction-dependent effective masses, are of pronounced interest for their roles in excitonic and magneto-optical phenomena. A perpendicular magnetic field complicates the separation of center-of-mass (c.m.) and relative motions, especially when electron and hole masses are comparable. Conventional theories often employ an approximate c.m. separation using factorized wave functions, modifying magnetic Hamiltonian terms and possibly introducing inaccuracies in magnetoexciton energy predictions. This work develops an exact analytical framework for c.m. and relative motion separation in anisotropic 2D magnetoexcitons, without resorting to the stationary-c.m. approximation. Starting from the full electron-hole Hamiltonian in a homogeneous magnetic field, the formalism uses the conserved pseudomomentum to derive a relative-motion Hamiltonian, revealing new anisotropy-dependent couplings and magnetic coefficients absent in approximate models. The resulting Schrödinger equation is treated via the Feranchuk-Komarov operator method and Levi-Civita transformation, allowing non-perturbative, systematically convergent solutions. Application to monolayer black phosphorus and titanium trisulfide, both freestanding and encapsulated in hexagonal boron nitride, yields magnetoexciton energies, diamagnetic coefficients, and probability densities for the ten lowest states across considerable magnetic-field ranges. The results demonstrate the significant influence of anisotropy-dependent coupling on magnetic response in systems with strong mass anisotropy. This formalism is generalizable to other anisotropic 2D semiconductors, establishing a foundation for advanced magneto-optical studies.

Keywords: Magnetoexciton, energies and wave functions, black phosphorus, titanium trisulfide, anisotropic 2D materials, exact center-of-mass separation, FK operator method

I. INTRODUCTION

The exploration of two-dimensional (2D) van der Waals materials has revealed a wide range of electronic and optical properties governed by strong Coulomb interactions and reduced dielectric screening [1–9]. In many 2D semiconductors, excitons dominate the optical response due to their large binding energies [10–22]. While numerous studies have focused on isotropic systems, many low-symmetry 2D materials exhibit pronounced in-plane anisotropy, resulting in direction-dependent effective masses and strongly anisotropic excitonic properties [23–29]. Recent surveys indicate that effective mass anisotropy is a widespread feature in two-dimensional materials [28, 29]. Such anisotropy plays an important role in determining polarization-dependent absorption, carrier dynamics, and magneto-optical responses in materials such as monolayer black phosphorus (BP) and titanium trisulfide (TiS₃) [30–43]. These unique properties make them promising for applications in electronic devices, polarization-resolved optics, and magneto-optical spectroscopy [44–48].

Magnetoexciton spectroscopy provides a powerful tool to probe effective masses, screening lengths, surrounding dielectric constants, and excitonic structure in 2D semiconductors [13–21]. Recent high-field magneto-optical

measurements in anisotropic and low-symmetry two-dimensional materials have further demonstrated the sensitivity of exciton energies and diamagnetic shifts to strong magnetic fields, highlighting the need for quantitatively reliable theoretical models [7, 9]. In isotropic systems, the exciton energy spectrum in a perpendicular magnetic field follows a well-established picture: rotational symmetry preserves magnetic quantum numbers, and the magnetic field dependence of exciton energies encodes the competition between magnetic confinement and the Coulomb attraction, described by the Rytova-Keldysh potential [49, 50]. In anisotropic 2D materials, however, the loss of rotational symmetry can lead to hybridization between angular-momentum channels and direction-dependent diamagnetic shifts, which consequently non-trivially modify both energy spectra and wave functions. Therefore, accurate theoretical descriptions are essential for quantitatively interpreting experimental data and extracting material parameters from magnetoexciton energies.

A fundamental aspect of the magnetoexciton problem is the separation of center-of-mass (c.m.) and relative motions. In homogeneous magnetic fields, these degrees of freedom are coupled, and the separation is nontrivial. For isotropic systems, rigorous treatments based on the conserved pseudomomentum provide an exact procedure

for isolating relative motion [51–55]. In anisotropic materials, where effective masses differ along principal directions, additional coupling terms arise in the Hamiltonian and modify magnetic-field-dependent contributions. In several theoretical studies of anisotropic magnetoexcitons [42, 43], the c.m. separation has been performed approximately by assuming that the total wave function factorizes into independent c.m. and relative components. This assumption is formally justified in electron–nucleus systems, where the nuclear mass dominates over the electron mass [56]. This approach simplifies the calculations and enables the practical evaluation of magnetoexciton energies. However, for excitons, when the electron and hole effective masses are comparable, the magnetic-field-induced coupling between c.m. and relative coordinates may modify the structure of the effective Hamiltonian. Therefore, a careful and systematic treatment of the c.m. separation is required in order to obtain quantitatively reliable magnetoexciton energies and diamagnetic coefficients. This issue becomes particularly relevant in the interpretation of high-field magneto-optical spectra, where small deviations in the magnetic coefficients may lead to noticeable differences in the extracted material parameters.

In the present work, we derive an exact analytical procedure for separating the c.m. and relative motions of an anisotropic two-dimensional exciton in a perpendicular magnetic field without invoking the stationary-c.m. approximation. Starting from the full electron–hole Hamiltonian, we employ the conserved pseudomomentum to construct the transformed relative-motion Hamiltonian. The resulting equation contains anisotropy-dependent coupling terms and modified magnetic coefficients that directly affect the magnetic contribution to the exciton binding energy. Our study considers the isotropic electron-hole interaction; however, the formalism can also be applied to materials with additional anisotropy in permittivity. In this case, the electron-hole interaction should instead be described by the anisotropic Keldysh potential [57].

To obtain numerical solutions, we solve the corresponding Schrödinger equation using the Feranchuk–Komarov (FK) operator method [58, 59] combined with the application of the Levi-Civita transformation [60]. This non-perturbative approach yields systematically convergent solutions with controllable precision, allowing accurate determination of magnetoexciton energies and wave functions. We apply the formalism to monolayer BP and TiS_3 in both freestanding (FS) and hexagonal boron nitride (hBN)-encapsulated environments. Magnetoexciton energies, diamagnetic coefficients, and probability densities are calculated over a broad magnetic-field range for the ten lowest excitonic states, and comprehensive numerical data tables are provided. These results provide a consistent and reproducible reference for future theoretical and experimental investigations of anisotropic magnetoexcitons.

The rest of the paper is organized as follows. In Sec. II we present the anisotropic electron–hole Hamiltonian and derive the exact c.m. separation and the resulting relative-motion equation. In Sec. III we outline the computational method, discuss the labeling of quantum states in anisotropic systems, and present numerical results for magnetoexciton energies and wave functions. Section IV summarizes the main findings and outlines possible extensions of the present formalism.

II. THE SCHRÖDINGER EQUATION FOR AN ANISOTROPIC 2D MAGNETOEXCITON

A. Hamiltonian of electron–hole system in a homogeneous magnetic field

We consider an exciton composed of an electron and a hole, confined in a two-dimensional plane, that interact via the Rytova-Keldysh potential [49, 50] in the presence of a perpendicular magnetic field \mathbf{B} applied perpendicular to the monolayer plane. The x and y directions are chosen to coincide with the principal axes of the effective mass tensor. The Hamiltonian of the system can be written as

$$\begin{aligned} \hat{H} = & \frac{1}{2m_x^e} (\hat{p}_x^e + eA_x^e)^2 + \frac{1}{2m_y^e} (\hat{p}_y^e + eA_y^e)^2 \\ & + \frac{1}{2m_x^h} (\hat{p}_x^h - eA_x^h)^2 + \frac{1}{2m_y^h} (\hat{p}_y^h - eA_y^h)^2 \\ & + V_{RK}(|\mathbf{r}_e - \mathbf{r}_h|), \end{aligned} \quad (1)$$

where m_x^e , m_y^e , m_x^h , and m_y^h denote the effective masses of the electron and hole along the x and y directions, respectively. Due to anisotropy, the effective masses in the two principal directions are different. The operators \hat{p}_x^e , \hat{p}_y^e , \hat{p}_x^h , \hat{p}_y^h represent the momentum components of the electron and hole. The interaction potential V_{RK} depends only on the relative coordinate $|\mathbf{r}_e - \mathbf{r}_h|$. Here, e is the magnitude of the electron charge and B is the magnetic field strength. Because the electron-hole interaction is still isotropic, it is better to adopt the symmetric gauge for the magnetic vector potential, whose components are given by $A_x^e = -By_e/2$, $A_y^e = +Bx_e/2$, $A_x^h = +By_h/2$, and $A_y^h = -Bx_h/2$.

To reduce the number of variables in Eq. (1) and separate collective and internal motions, we introduce relative and center-of-mass coordinates

$$\begin{aligned} x &= x_e - x_h, & y &= y_e - y_h, \\ X &= \frac{m_x^e x_e + m_x^h x_h}{m_x^e + m_x^h}, & Y &= \frac{m_y^e y_e + m_y^h y_h}{m_y^e + m_y^h}. \end{aligned} \quad (2)$$

After performing the coordinate transformation and carrying out the corresponding algebraic manipulations, the Hamiltonian expressed in the variables (x, y, X, Y) takes

the form

$$\hat{H} = \frac{1}{2M_x} \hat{P}_X^2 + \frac{1}{2M_y} \hat{P}_Y^2 + \frac{1}{2\mu_x} \hat{p}_x^2 + \frac{1}{2\mu_y} \hat{p}_y^2 + \hat{H}_B + V_{RK}(r), \quad (3)$$

where \hat{H}_B is the magnetic-field-dependent contribution, and the effective masses are defined as

$$M_x = m_x^e + m_x^h, \quad M_y = m_y^e + m_y^h, \\ \mu_x = \frac{m_x^e m_x^h}{m_x^e + m_x^h}, \quad \mu_y = \frac{m_y^e m_y^h}{m_y^e + m_y^h}. \quad (4)$$

Here, M_x and M_y represent the c.m. masses along the two principal directions, while μ_x and μ_y are the corresponding reduced masses for the relative motion. The operators \hat{P}_X and \hat{P}_Y denote the c.m. momentum components, and \hat{p}_x and \hat{p}_y represent the relative-motion momenta. The relative distance is given by $r = \sqrt{x^2 + y^2}$.

The magnetic-field-dependent contribution consists of linear and quadratic terms in the magnetic field B as $\hat{H}_B = \hat{H}_{\text{lin}} + \hat{H}_{\text{quad}}$, where

$$\hat{H}_{\text{lin}} = \frac{eB}{2} \left[\left(\frac{m_y^e}{m_x^h} - \frac{m_y^h}{m_x^e} \right) \frac{y}{M_y} \hat{p}_x - \frac{y}{M_x} \hat{P}_x - \frac{Y}{\mu_x} \hat{p}_x - \left(\frac{m_x^e}{m_y^h} - \frac{m_x^h}{m_y^e} \right) \frac{x}{M_x} \hat{p}_y + \frac{x}{M_y} \hat{P}_y + \frac{X}{\mu_y} \hat{p}_y \right]$$

and

$$\hat{H}_{\text{quad}} = -\frac{e^2 B^2}{8} \left[\frac{X^2}{\mu_y} + \left(\frac{m_x^h}{m_y^2} + \frac{m_x^e}{m_y^h} \right) \frac{x^2}{M_x^2} + \left(\frac{m_x^h}{m_y^e} - \frac{m_x^e}{m_y^h} \right) \frac{2xX}{M_x} + \left(\frac{m_y^h}{m_x^2} - \frac{m_y^e}{m_x^h} \right) \frac{2yY}{M_y} + \frac{Y^2}{\mu_x} + \left(\frac{m_y^h}{m_x^2} + \frac{m_y^e}{m_x^h} \right) \frac{y^2}{M_y^2} \right].$$

The Hamiltonian clearly contains coupling terms between the relative and c.m. coordinates. Therefore, the variables cannot be separated in a straightforward manner, and a more careful transformation is required. This exact separation procedure will be presented in the next subsection.

B. Exact center-of-mass separation

To proceed with the analysis, it is necessary to separate the c.m. and relative motions from the Hamiltonian (3). In the presence of a homogeneous magnetic field, however, this separation is nontrivial because the c.m. and relative coordinates are coupled through the magnetic term \hat{H}_B . In particular, the canonical momentum associated with the c.m. motion is no longer conserved due to the vector potential.

Nevertheless, the system possesses a conserved quantity known as the *pseudomomentum* [51, 52], represented by an operator defined as

$$\hat{\mathbf{P}}_0 = \hat{\mathbf{P}} - \frac{1}{2} e \mathbf{B} \times \mathbf{r}, \quad (5)$$

where $\mathbf{P} = P_X \mathbf{i} + P_Y \mathbf{j}$ is the total canonical momentum and $\mathbf{r} = x \mathbf{i} + y \mathbf{j}$ is the relative coordinate. It can be verified directly that $[\hat{\mathbf{P}}_0, \hat{H}] = 0$, which implies that $\hat{\mathbf{P}}_0$ and \hat{H} share a common set of eigenfunctions. We therefore seek solutions of the form

$$\Psi(\mathbf{r}, \mathbf{R}) = \exp \left[\frac{i}{\hbar} (\mathbf{K} + \frac{1}{2} e \mathbf{B} \times \mathbf{r}) \cdot \mathbf{R} \right] \psi(\mathbf{r}), \quad (6)$$

where $\mathbf{R} = X \mathbf{i} + Y \mathbf{j}$, and $\mathbf{K} = K_x \mathbf{i} + K_y \mathbf{j}$ is the eigenvalue of the pseudomomentum operator. Substituting Eq. (6) into the Schrödinger equation and performing the unitary transformation $\hat{U} = \exp \left[\frac{i}{\hbar} (\mathbf{K} + \frac{1}{2} e \mathbf{B} \times \mathbf{r}) \cdot \mathbf{R} \right]$, we obtain

$$\hat{U}^{-1} \hat{H} \hat{U} \psi(x, y) = E \psi(x, y). \quad (7)$$

The relative-motion Hamiltonian is then defined as

$$\hat{H}_{\text{rel}} = \hat{U}^{-1} \hat{H} \hat{U} - \frac{1}{2M_x} K_x^2 - \frac{1}{2M_y} K_y^2, \quad (8)$$

where the subtracted terms correspond to the kinetic energy of the c.m. motion.

Carrying out the transformation explicitly, we obtain the relative-motion Hamiltonian in the form

$$\hat{H}_{\text{rel}} = -\frac{\hbar^2}{2\mu_x} \frac{\partial^2}{\partial x^2} - \frac{\hbar^2}{2\mu_y} \frac{\partial^2}{\partial y^2} + \frac{e^2 B^2}{8} \left(\frac{\beta_y + \alpha^2}{\mu_y} x^2 + \frac{\beta_x + \alpha^2}{\mu_x} y^2 \right) - i\hbar \alpha \frac{eB}{2} \left(\frac{y}{\mu_y} \frac{\partial}{\partial x} - \frac{x}{\mu_x} \frac{\partial}{\partial y} \right) + V_{RK}(r) + \frac{eB}{M_x} K_y x - \frac{eB}{M_y} K_x y, \quad (9)$$

where the dimensionless coefficients are defined as

$$\alpha = \frac{1 - \rho_x \rho_y}{(1 + \rho_x)(1 + \rho_y)}, \\ \beta_x = \frac{4\rho_x}{(1 + \rho_x)^2}, \quad \beta_y = \frac{4\rho_y}{(1 + \rho_y)^2}, \quad (10)$$

with mass ratios $\rho_x = m_x^e/m_x^h$ and $\rho_y = m_y^e/m_y^h$.

Equation (9) represents the exact relative-motion Hamiltonian for an anisotropic two-dimensional magnetoexciton. The anisotropy is reflected in both the kinetic terms through the reduced masses μ_x and μ_y , and the magnetic contributions through the coefficients α , β_x , and β_y . The presence of the linear derivative term proportional to α indicates the magnetic-field-induced coupling between different angular components of the wave

function. The quadratic magnetic terms contain modified coefficients that are properly reduced to unity in the isotropic limit.

Thus, without invoking any stationary-c.m. approximation, we obtain an exact separation of the c.m. motion and a closed Schrödinger equation (9) for the relative motion of the anisotropic magnetoexciton.

C. The Schrödinger for relative motion

In Eq. (9), the relative-motion Hamiltonian contains terms proportional to the pseudomomentum components K_x and K_y . These terms describe the coupling between the relative motion and the c.m. motion in the presence of a magnetic field. In general, the exciton c.m. may carry finite momentum determined by thermal excitation or external perturbations. For a thermalized exciton ensemble, the kinetic energy of the c.m. motion can be estimated as $k_B T$, where k_B is the Boltzmann constant and T is the temperature. Using the equipartition theorem

$$\frac{1}{2M_x} K_x^2 \sim k_B T, \quad \frac{1}{2M_y} K_y^2 \sim k_B T,$$

one obtains characteristic values

$$K_x \sim \sqrt{2M_x k_B T}, \quad K_y \sim \sqrt{2M_y k_B T}.$$

In typical low-temperature magneto-optical experiments on 2D semiconductors, the exciton c.m. momentum is small [55]. Therefore, in the following analysis, we focus on the case $K_x = K_y = 0$, which corresponds to excitons near the bottom of the dispersion and captures the dominant contribution to optical transitions. Under this condition, the Schrödinger equation for relative motion becomes

$$\left\{ -\frac{1}{2\mu_x} \frac{\partial^2}{\partial x^2} - \frac{1}{2\mu_y} \frac{\partial^2}{\partial y^2} - i \frac{\alpha B}{2} \left(\frac{y}{\mu_x} \frac{\partial}{\partial x} - \frac{x}{\mu_y} \frac{\partial}{\partial y} \right) + \frac{B^2}{8} \left(\frac{\beta_y + \alpha^2}{\mu_y} x^2 + \frac{\beta_x + \alpha^2}{\mu_x} y^2 \right) + V_{RK}(r) \right\} \psi(x, y) = E \psi(x, y), \quad (11)$$

where we have expressed the equation in atomic units. In these units, energies are measured in Hartree energy E_H , distances in Bohr radius a_0 , and the magnetic field in units of $B_0 = (m_e/e\hbar)E_H = 23\,051.7$ tesla (T). The reduced masses μ_x and μ_y are given in units of the electron mass m_e .

The interaction potential $V_{RK}(r)$ remains isotropic, as the dielectric screening of the surrounding medium is assumed to be isotropic. For the numerical calculations presented below, we employ the Rytova-Keldysh potential expressed in the Fourier representation,

$$V_{RK}(r) = -\frac{1}{2\pi\kappa} \int_{-\infty}^{+\infty} \int_{-\infty}^{+\infty} dq_1 dq_2 \frac{e^{iq_1 x + iq_2 y}}{q(1 + \frac{r_0}{\kappa} q)}, \quad (12)$$

where $q = \sqrt{q_1^2 + q_2^2}$, r_0 is the screening length (in units of Bohr radius a_0), and κ is the surrounding dielectric constant.

In contrast to the isotropic case, where alternative representations, such as the Laplace transform given in [19], may be convenient, the Fourier representation (12) is particularly suitable for anisotropic systems because it preserves the explicit dependence on Cartesian coordinates x and y . Equation (11) therefore provides a starting point for the numerical solution of the anisotropic magnetoexciton problem.

D. Comparison with previous treatments

The Schrödinger equation for relative motion derived in Eq. (11) differs from those obtained in earlier studies [42, 43] employing approximate c.m. separation procedures. In the present formulation, additional anisotropy-dependent terms appear explicitly in the relative-motion Hamiltonian.

First, Eq. (11) contains the Zeeman term

$$\hat{H}_{Zeeman} = -i \frac{\alpha B}{2} \left(\frac{y}{\mu_x} \frac{\partial}{\partial x} - \frac{x}{\mu_y} \frac{\partial}{\partial y} \right), \quad (13)$$

which is absent in treatments based on factorized wave functions for the s states. This term (13) is associated with the orbital motion of the electron-hole pair and is correctly reduced to the known isotropic limit [19] when $\mu_x = \mu_y = \mu$ and $\rho_x = \rho_y = \rho$. In this limit, $\alpha = (1 - \rho)/(1 + \rho)$, and the term becomes a coupling between the magnetic field and the angular momentum. In anisotropic systems, where angular momentum is no longer conserved, this contribution reflects the mixing of different angular components induced by the magnetic field and effective-mass anisotropy. In the calculations presented here, this term is retained for all states.

Second, the diamagnetic term

$$\hat{H}_{diamag} = \frac{e^2 B^2}{8} \left(\frac{\beta_y + \alpha^2}{\mu_y} x^2 + \frac{\beta_x + \alpha^2}{\mu_x} y^2 \right) \quad (14)$$

contains coefficients $\beta_x + \alpha^2$ and $\beta_y + \alpha^2$ determined by the exact transformation. In the isotropic limit, these coefficients reduce to unity, recovering the standard form of the magnetic confinement term, presented in [19]. In anisotropic materials, however, their values depend explicitly on the mass ratios ρ_x and ρ_y by Eqs. (10). The commonly used approximation, based on the assumption that the wave function factorizes as $\Psi(\mathbf{r}, \mathbf{R}) = \exp(\frac{i}{\hbar} \mathbf{K} \cdot \mathbf{R}) \psi(\mathbf{r})$ as suggested in Ref. [56], corresponds effectively to the limit of a much heavier hole mass, where $\rho_x, \rho_y \rightarrow 0$, leading to $\beta_x + \alpha^2 = 1$ and $\beta_y + \alpha^2 = 1$.

For realistic material parameters of BP and TiS₃ presented in Table I, the coefficients deviate from unity, as shown in Table II. These deviations reflect the intrinsic mass anisotropy and directly influence the magnetic

TABLE I. Electron and hole effective masses m_x^e , m_y^e , m_x^h , and m_y^h (m_e) in monolayer black phosphorus (BP) and titanium trisulfide (TiS₃) from Refs. [35–37], together with the calculated exciton reduced masses μ_x and μ_y (m_e).

	m_x^e	m_y^e	m_x^h	m_y^h	μ_x	μ_y
BP	0.199	0.753	0.168	5.353	0.091	0.660
TiS ₃	1.52	0.40	0.30	0.99	0.251	0.285

TABLE II. Coefficients α , $\beta_x + \alpha^2$, and $\beta_y + \alpha^2$ in Eqs. (13) and (14) calculated using the exact theoretical formulas (10) for BP and TiS₃.

	ρ_x	ρ_y	α	$\beta_x + \alpha^2$	$\beta_y + \alpha^2$
BP	1.176	0.140	0.337	1.107	0.545
TiS ₃	5.067	0.404	-0.123	0.566	0.835

contribution to the exciton energy and the calculated diamagnetic coefficients. Therefore, retaining the exact coefficients ensures internal consistency of the Hamiltonian and provides a quantitatively reliable description of anisotropic magnetoexcitons.

III. NUMERICAL RESULTS FOR MAGNETOEXCITON ENERGIES

A. Method of calculations

To solve the relative-motion Schrödinger equation (11), we employ the FK operator method [58, 59] combined with the application of the Levi-Civita transformation [60]. This approach provides a non-perturbative and algebraic framework suitable for anisotropic systems and allows systematically convergent numerical solutions with controllable precision.

First, we perform the Levi-Civita transformation

$$x = u^2 - v^2, \quad y = 2uv, \quad (15)$$

which maps the original two-dimensional problem into a form analogous to a two-dimensional anharmonic oscillator. This transformation is particularly convenient for treating Coulomb-type interactions and has been successfully applied in related excitonic systems [14, 19, 21, 55].

In the transformed (u, v) space, the Hamiltonian can be expressed in terms of creation and annihilation operators,

$$\hat{a}(\omega) = \sqrt{\frac{\omega}{2}} \left(u + \frac{1}{\omega} \frac{\partial}{\partial u} \right), \quad \hat{a}^+(\omega) = \sqrt{\frac{\omega}{2}} \left(u - \frac{1}{\omega} \frac{\partial}{\partial u} \right),$$

$$\hat{b}(\omega) = \sqrt{\frac{\omega}{2}} \left(v + \frac{1}{\omega} \frac{\partial}{\partial v} \right), \quad \hat{b}^+(\omega) = \sqrt{\frac{\omega}{2}} \left(v - \frac{1}{\omega} \frac{\partial}{\partial v} \right),$$

where ω is a variational parameter that can be adjusted to optimize convergence. The operators satisfy the commutation relation $[\hat{a}, \hat{a}^+] = 1$ and $[\hat{b}, \hat{b}^+] = 1$.

Next, the wave function is expanded in the complete basis set

$$|jk\rangle = \frac{1}{\sqrt{(j-k)!(j+k)!}} (\hat{a}^+)^{j+k} (\hat{b}^+)^{j-k} |0(\omega)\rangle, \quad (16)$$

where the vacuum state is defined by equations $\hat{a}|0\rangle = 0$ and $\hat{b}|0\rangle = 0$; quantum number j is a non-negative number $j = 0, 1, 2, \dots$, while k is an integer less than j : $k = -j, -j+1, \dots, +j$. The eigenfunction is written as

$$|\psi\rangle = \sum_{j=0}^{+\infty} \sum_{k=-j}^{+j} C_{jk} |jk\rangle. \quad (17)$$

Substituting this expansion into the Schrödinger equation reduces the problem to a matrix eigenvalue equation for the coefficients C_{jk} . All matrix elements are evaluated analytically using algebraic manipulation of the operator commutation relations, resulting in an explicit finite-dimensional generalized eigenvalue problem.

In practical calculations, the basis set is truncated at $j \leq N_{\max}$. We typically use $N_{\max} = 20$, which ensures that the lowest excitonic energies converge to the desired precision. The convergence was verified by increasing N_{\max} and monitoring the stability of the eigenvalues. Variations of the parameter ω were also examined to confirm that the resulting energies are insensitive to this parameter choice within an appropriate range. These checks guarantee that the obtained solutions are systematically convergent and numerically stable.

The resulting matrix eigenvalue problem is solved using standard linear algebra routines (e.g., the Linear Algebra Package (LAPACK) [61] or equivalent numerical libraries). This procedure yields magnetoexciton energies and wave functions with controlled numerical accuracy for the anisotropic systems considered.

B. Labeling the quantum states

In anisotropic systems, the magnetic quantum number is no longer a conserved quantity because rotational symmetry is broken. Nevertheless, it is convenient to retain the conventional notation s , p_x , p_y , etc., in order to facilitate comparison with the isotropic limit and with previous studies.

In the present work, the labeling of quantum states is performed on the basis of the structure of the eigenvectors obtained from the expansion (17). After solving the matrix eigenvalue problem, each eigenstate is characterized by a set of coefficients C_{jk} . The contribution of each basis state $|jk\rangle$ to a given eigenfunction is determined by the magnitude of the corresponding coefficient. The dominant component provides a natural way to assign approximate quantum numbers (n, m) to the state.

In particular, the states labeled as “s” correspond to those whose dominant contribution originates from basis states with $k = 0$. Similarly, the states p_x and p_y

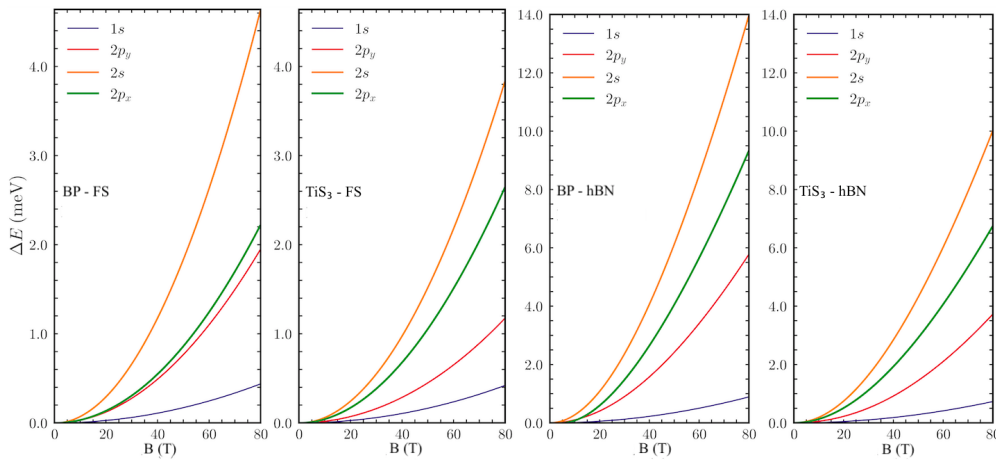


FIG. 1. (Color online) Magnetic contribution to the exciton binding energy as a function of the magnetic field B : $\Delta E = E(B) - E(B = 0)$ for the states $1s$, $2p_y$, $2p_x$, $2s$ with $r_0=2.576$ nm (for BP), $r_0=4.434$ nm (for TiS_3), $\kappa = 1.0$ (for FS), and $\kappa = 4.9$ (for hBN).

are associated with dominant contributions from components corresponding to $k = +1$ and $k = -1$, respectively. Because of anisotropy and magnetic-field-induced coupling, eigenfunctions (17) generally contain admixtures of several angular components; therefore, labels should be understood as approximate classifications rather than exact quantum numbers.

For highly excited states and for systems with strong anisotropy (large ratio $\beta = \mu_y/\mu_x$), the hybridization between the basis states in (17) becomes more pronounced. In such cases, the magnitudes of several coefficients C_{jk} may become comparable, making the identification less straightforward. To ensure consistent labeling, we track the evolution of eigenvalues by gradually varying the anisotropy parameter from the isotropic limit $\beta = 1$ to the physical value of the material under consideration. This procedure allows consistent identification of states across the full anisotropy range. Each state can thus be continuously connected to its counterpart in the isotropic case, where the quantum numbers are well-defined. This procedure allows for a systematic and unambiguous assignment of state labels throughout the calculations.

C. Magnetoexciton energies

We now present the numerical results for magnetoexciton energies obtained from the exact c.m. separation and the systematically convergent FK operator method described above. Calculations are performed for monolayer BP and TiS_3 in both FS and hBN-encapsulated configurations. The effective masses are taken from the references listed in Table I, the screening length values r_0 are 2.576 nm for BP [10] and 4.434 for TiS_3 [36], and the surrounding dielectric constant $\kappa = 1$ for FS environments, while the value $\kappa = 4.9$ for hBN-encapsulated slabs [4, 42].

As a consistency check, we first consider the case without a magnetic field ($B = 0$). The calculated exciton binding energies agree with previously reported theoretical values [37, 42] and are consistent with the experimental data available for freestanding BP [32, 38], as shown in Table III. This agreement supports the reliability of both the material parameters and the numerical implementation.

TABLE III. Calculated exciton energies (meV) in BP and TiS_3 compared with those in other theoretical and experimental studies for the case without magnetic field ($B = 0$).

	1s	2p _y	2s	2p _x
BP (freestanding)				
Our study	745.73	478.56	377.57	310.93
Theor. [42]	746.06	478.75	377.72	311.22
Exp. [38]	762	–	–	–
Exp. [32]	900 ± 120	–	–	–
(in hBN)				
Our study	199.01	74.06	50.13	31.83
Theor. [42]	199.66	74.37	50.35	32.03
TiS₃ (freestanding)				
Our study	537.45	314.24	306.85	255.64
Theor. [37]	537.1	–	–	–

The primary focus of the present work is the magnetic-field dependence of exciton energies. Magnetoexciton energies are computed over a broad magnetic-field range up to 120 T for the ten lowest excitonic states. The complete numerical values are provided in Tables VII–VIII of the Appendix A, offering a comprehensive dataset for anisotropic magnetoexciton spectra.

Figure 1 illustrates the magnetic contribution to the binding energy $\Delta E(B) = E(B) - E(B = 0)$ for the four lowest states ($1s$, $2p_y$, $2s$, and $2p_x$). The magnetic-field dependence reflects the interplay between anisotropic ef-

TABLE IV. Diamagnetic coefficients in BP and TiS_3 monolayers, calculated by our method with the exact c.m. separation compared with those of Refs. [42, 43].

State	BP				TiS_3			
	Our work		Ref. [42]		Our work		Ref. [43]	
	hBN	FS	hBN	FS	hBN	FS	hBN	FS
1	0.14	0.07	0.46	0.21	0.11	0.07	0.17	0.095
2	1.02	0.31	1.41	0.40	0.56	0.18	—	0.04
3	2.70	0.74	2.96	0.67	1.27	0.43	—	0.46
4	—	0.34	—	1.88	1.87	0.61	—	0.88

fective masses and magnetic confinement. In strongly anisotropic materials such as BP, the deviations from isotropic behavior become more pronounced, particularly for excited states. In contrast, for TiS_3 , where the mass anisotropy is weaker, the magnetic response exhibits a comparatively smoother evolution.

The diamagnetic coefficients are extracted from the low-field quadratic behavior,

$$\sigma_{\text{diamag}} = \frac{1}{2} \lim_{B \rightarrow 0} \frac{\partial^2 E(B)}{\partial B^2}, \quad (18)$$

and are summarized in Table IV. The observed differences between the present values and those reported in Refs. [42, 43] are likely related to differences in the treatment of c.m. separation and magnetic coupling terms in anisotropic systems. The results show that anisotropy-dependent coupling terms significantly influence the diamagnetic response, especially in BP. Since these coefficients determine the curvature of the energy shift at low magnetic fields, their accurate evaluation is essential for the quantitative interpretation of magneto-optical measurements.

The availability of systematic numerical data for ten excitonic states, presented in Tables VII–VIII, enables detailed analysis of higher excited states, whose magnetic evolution is sensitive to both effective-mass anisotropy and screening effects. These results provide a consistent and reproducible reference for future theoretical modeling and comparison with high-field magneto-optical experiments.

D. Wave functions

To obtain a more comprehensive understanding of how the surrounding environment influences the exciton’s spatial distribution, we compute wave functions and visualize the corresponding probability densities for the following scenarios. First, we consider the anisotropy case, keeping the magnetic field fixed at $B = 0$. Second, we include both anisotropy and a finite magnetic field. The results are shown for TiS_3 for the four excitonic states 1s, 2s, $2p_x$, and $2p_y$. The purpose of this analysis is to examine how the exciton probability density evolves

across different environments, starting from the case with only anisotropy and progressing to the case with both anisotropy and a magnetic field. We can see that, although the anisotropy of TiS_3 is relatively low, its influence on the electron distributions is significant, as shown in Fig. 2 for TiS_3 encapsulated by hBN. A similar scenario for BP is presented in Fig. 3.

As mentioned above, we label the first four states by 1s, 2s, $2p_x$, $2p_y$, while other theoretical studies label them as 1s, 2s, 3s, and 4s [37, 42, 43]. For genuine quasi-s states, the wave function must satisfy $|\psi(0)|^2 \neq 0$. In contrast, for states with an azimuthal quantum number $m \neq 0$, we have $|\psi(0)|^2 = 0$. The electron distributions given in Figs. 2 and 3 demonstrate that our definitions are more appropriate.

IV. CONCLUSION

In this work, we have derived an exact analytical procedure for separating the center-of-mass (c.m.) and relative motions of an anisotropic two-dimensional exciton in a perpendicular magnetic field. By employing the conserved pseudomomentum, we obtained a relative-motion Hamiltonian that explicitly contains anisotropy-dependent coupling terms and modified magnetic coefficients arising from direction-dependent effective masses. These terms influence the magnetic contribution to the exciton binding energy and the associated diamagnetic response.

The resulting Schrödinger equation was solved using the Feranchuk–Komarov operator method combined with the Levi-Civita transformation. This non-perturbative approach provides systematically convergent numerical solutions with controllable precision, enabling accurate determination of magnetoexciton energies and wave functions in anisotropic systems.

Applying the formalism to monolayer black phosphorus and titanium trisulfide in both freestanding and hBN-encapsulated configurations, we calculated magnetoexciton energies, diamagnetic coefficients, and probability densities for the ten lowest excitonic states over a broad range of magnetic fields. The comprehensive numerical data tables presented in this work provide a consistent and reproducible reference for anisotropic magnetoexciton spectra and may serve as benchmarks for future theoretical and magneto-optical investigations.

The formalism developed here is general and can be extended to other anisotropic 2D semiconductors and heterostructures. Possible directions for further study include finite pseudomomentum effects at elevated temperatures, excitonic complexes such as trions and biexcitons, and strain-induced anisotropy. The present results contribute to a systematic theoretical framework for magnetoexcitons in low-symmetry two-dimensional materials.

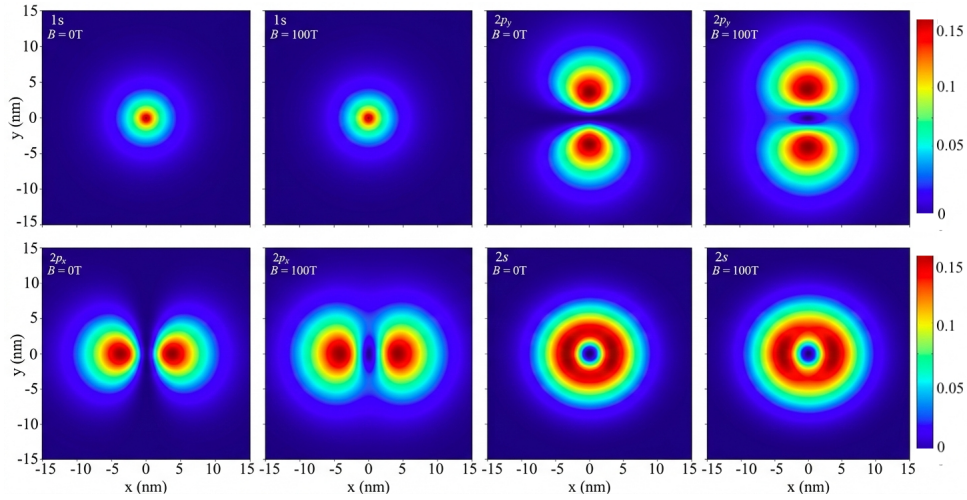


FIG. 2. (Color online) The probability density for a magnetoexciton in TiS_3 .

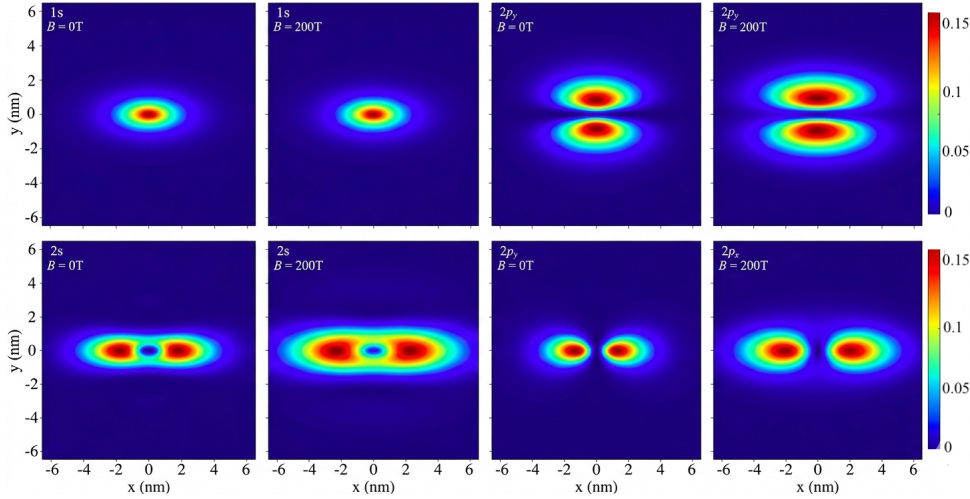


FIG. 3. (Color online) The probability density for a magnetoexciton in BP.

ACKNOWLEDGMENTS

This research is funded by Vietnam Ministry of Education and Training, Grant number B2025-SPS-03 and carried out by the high-performance cluster at Ho Chi Minh City University of Education, Vietnam.

Contribution: V.-H.L. and D.-K.D.L. conceptualized the work, developed the methodology, and performed analytical formulation; D.-K.D.L. and H.-V.L. carried out

numerical calculations; V.-H.L., D.-K.D.L., and D.-N.L. analyzed the data and contributed to the interpretation of the physical underlying; H.-V.L., D.-A.P.N., T.-S.N., and N.-T.D.H. validated the data; V.-H.L., D.-K.D.L., and D.-N.L. wrote the original draft; N.-T.D.H. acquired the funding; V.-H.L. and N.-T.D.H. supervised the work. All authors discussed the results and contributed to the review, editing, and finalization of the manuscript.

Appendix A: Magnetoexciton energies

For completeness and reproducibility, we list the calculated magnetoexciton energies for the ten lowest states at magnetic field intensities up to 120 T for monolayer black phosphorus (BP) and titanium trisulfide (TiS_3), considering both freestanding and hexagonal boron nitride (hBN)-encapsulated environments.

TABLE V. Magnetoexciton energies in monolayer BP in FS with $r_0 = 2.576$ nm, $\mu_x = 0.091 m_e$, $\kappa = 1.0$ and $\beta = 7.249$.

Magnetic field (T)	Energy (meV)									
	1s	2p _y	2s	2p _x	3p _y	3s	3d _y	4s	3p _x	4p _y
0	-745.738	-478.564	-377.573	-310.933	-297.502	-250.417	-233.884	-207.986	-196.664	-192.115
2	-745.738	-478.564	-377.573	-310.933	-297.502	-250.417	-233.884	-207.986	-196.664	-192.115
4	-745.737	-478.560	-377.565	-310.929	-297.484	-250.390	-233.872	-207.940	-196.647	-192.089
6	-745.736	-478.554	-377.550	-310.922	-297.452	-250.344	-233.852	-207.863	-196.618	-192.046
8	-745.734	-478.545	-377.529	-310.913	-297.409	-250.281	-233.823	-207.756	-196.578	-191.985
10	-745.732	-478.534	-377.502	-310.901	-297.353	-250.200	-233.787	-207.618	-196.527	-191.907
20	-745.711	-478.442	-377.281	-310.798	-296.888	-249.530	-233.482	-206.481	-196.106	-191.257
30	-745.677	-478.288	-376.912	-310.627	-296.118	-248.435	-232.967	-204.631	-195.426	-190.175
40	-745.629	-478.074	-376.398	-310.386	-295.052	-246.950	-232.231	-202.135	-194.508	-188.660
60	-745.492	-477.463	-374.943	-309.690	-292.070	-243.028	-229.990	-195.612	-192.025	-184.254
70	-745.403	-477.068	-374.006	-309.235	-290.179	-240.750	-228.394	-191.864	-190.482	-181.255
80	-745.300	-476.614	-372.935	-308.710	-288.038	-238.400	-226.389	-188.747	-188.025	-177.606
90	-745.184	-476.103	-371.732	-308.115	-285.660	-236.088	-223.898	-186.827	-184.247	-173.231
100	-745.054	-475.535	-370.401	-307.450	-283.057	-233.893	-220.875	-184.728	-180.595	-168.138
120	-744.755	-474.231	-367.372	-305.921	-277.227	-229.909	-213.307	-180.014	-173.553	-156.166

TABLE VI. Magnetoexciton energies in monolayer BP in hBN with $r_0 = 2.576$ nm, $\mu_x = 0.091 m_e$, $\kappa = 4.9$ and $\beta = 7.249$.

Magnetic field (T)	Energy (meV)									
	1s	2p _y	2s	2p _x	3p _y	3s	3d _y	4s	3p _x	4p _y
0	-199.011	-74.065	-50.139	-31.836	-31.419	-23.921	-17.974	-14.356	-12.691	-12.425
2	-199.011	-74.060	-50.128	-31.840	-31.377	-23.882	-17.954	-14.320	-12.703	-12.323
4	-199.009	-74.048	-50.095	-31.842	-31.261	-23.765	-17.894	-14.212	-12.682	-12.075
6	-199.006	-74.028	-50.039	-31.832	-31.082	-23.573	-17.794	-14.035	-12.588	-11.721
8	-199.002	-73.999	-49.962	-31.803	-30.848	-23.308	-17.651	-13.790	-12.415	-11.270
10	-198.997	-73.962	-49.863	-31.755	-30.562	-22.973	-17.466	-13.479	-12.163	-10.724
20	-198.955	-73.658	-49.057	-31.240	-28.419	-20.523	-15.792	-11.069	-9.839	-6.625
30	-198.885	-73.162	-47.772	-30.356	-25.277	-17.748	-12.397	-7.590	-6.333	-3.179
40	-198.787	-72.487	-46.072	-29.186	-21.403	-15.385	-7.231	-3.445	-2.610	0.915
60	-198.508	-70.657	-41.652	-26.182	-12.184	-10.899	4.668	5.366	6.412	11.546
70	-198.328	-69.533	-39.025	-24.416	-8.536	-7.058	8.423	10.843	13.262	17.382
80	-198.121	-68.288	-36.170	-22.505	-6.071	-1.684	12.288	16.175	20.741	23.428
90	-197.888	-66.934	-33.114	-20.467	-3.510	3.888	16.255	21.627	28.437	29.642
100	-197.629	-65.483	-29.883	-18.316	-0.863	9.621	20.316	27.204	35.986	36.001
120	-197.034	-62.324	-22.968	-13.716	4.663	21.444	28.691	38.679	48.129	49.080

TABLE VII. Magnetoexciton energies in monolayer TiS₃ in FS with $r_0 = 4.434$ nm, $\mu_x = 0.251 m_e$, $\kappa = 1.0$ and $\beta = 1.135$.

Magnetic field (T)	Energy (meV)									
	1s	2p _y	2s	2p _x	3p _y	3s	3d _y	4s	3p _x	4p _y
0	-537.456	-314.242	-306.859	-255.647	-208.980	-208.655	-187.563	-181.891	-159.312	-150.324
2	-537.456	-314.242	-306.859	-255.647	-208.980	-208.655	-187.563	-181.892	-159.312	-150.324
4	-537.455	-314.240	-306.854	-255.640	-209.053	-208.563	-187.550	-181.872	-159.287	-150.464
6	-537.454	-314.236	-306.846	-255.627	-209.133	-208.451	-187.528	-181.839	-159.246	-150.589
8	-537.452	-314.231	-306.834	-255.610	-209.211	-208.328	-187.497	-181.793	-159.188	-150.702
10	-537.450	-314.225	-306.818	-255.588	-209.285	-208.197	-187.457	-181.734	-159.114	-150.802
20	-537.430	-314.172	-306.690	-255.404	-209.569	-207.435	-187.126	-181.244	-158.500	-151.102
30	-537.397	-314.083	-306.477	-255.099	-209.700	-206.510	-186.574	-180.437	-157.488	-151.082
40	-537.351	-313.957	-306.182	-254.674	-209.678	-205.431	-185.805	-179.325	-156.094	-150.754
60	-537.220	-313.592	-305.350	-253.468	-209.183	-202.821	-183.627	-176.249	-152.250	-149.238
80	-537.036	-313.067	-304.212	-251.808	-208.121	-199.643	-180.640	-172.149	-147.149	-146.695
90	-536.925	-312.742	-303.536	-250.813	-207.389	-197.855	-178.864	-169.757	-145.081	-144.186
100	-536.801	-312.375	-302.791	-249.713	-206.531	-195.941	-176.910	-167.157	-143.262	-140.978
120	-536.513	-311.513	-301.104	-247.212	-204.457	-191.758	-172.512	-161.392	-139.060	-133.899

TABLE VIII. Magnetoexciton energies in monolayer TiS_3 in FS with $r_0 = 4.434$ nm, $\mu_x = 0.251 m_e$, $\kappa = 4.9$ and $\beta = 1.135$.

Magnetic field (T)	Energy (meV)									
	1s	2p _y	2s	2p _x	3p _y	3s	3d _y	4s	3p _x	4p _y
0	-172.543	-54.571	-51.964	-41.138	-22.900	-22.882	-21.784	-20.605	-17.687	-11.562
2	-172.542	-54.569	-51.958	-41.130	-22.982	-22.769	-21.764	-20.575	-17.652	-11.685
4	-172.541	-54.562	-51.943	-41.108	-23.041	-22.615	-21.705	-20.485	-17.548	-11.738
6	-172.539	-54.551	-51.917	-41.070	-23.069	-22.431	-21.607	-20.336	-17.377	-11.721
8	-172.535	-54.536	-51.880	-41.017	-23.066	-22.217	-21.469	-20.130	-17.139	-11.636
10	-172.531	-54.516	-51.834	-40.949	-23.035	-21.973	-21.292	-19.870	-16.836	-11.485
20	-172.497	-54.348	-51.454	-40.391	-22.480	-20.357	-19.868	-17.875	-14.469	-9.876
30	-172.439	-54.061	-50.845	-39.494	-21.379	-18.197	-17.688	-14.984	-10.993	-7.223
40	-172.359	-53.651	-50.034	-38.293	-19.865	-15.626	-14.948	-11.475	-6.785	-3.961
60	-172.130	-52.469	-47.901	-35.120	-15.951	-9.601	-8.310	-3.219	3.007	3.601
80	-171.812	-50.844	-45.212	-31.116	-11.199	-2.744	-0.628	6.119	12.076	13.979
90	-171.620	-49.884	-43.695	-28.861	-8.591	0.913	3.488	11.061	16.569	19.767
100	-171.406	-48.835	-42.079	-26.461	-5.856	4.695	7.748	16.138	21.207	25.711
120	-170.915	-46.499	-38.584	-21.286	-0.067	12.571	16.616	26.583	30.887	37.973

- [1] A. K. Geim and I. V. Grigorieva, Van der Waals heterostructures, *Nature* **499**, 419 (2013).
- [2] A. Chernikov, T. C. Berkelbach, H. M. Hill, A. Rigosi, Y. Li, O. B. Aslan, D. R. Reichman, M. S. Hybertsen, and T. F. Heinz, Exciton binding energy and nonhydrogenic Rydberg series in monolayer WS_2 , *Phys. Rev. Lett.* **113**, 076802 (2014).
- [3] G. Wang, A. Chernikov, M. M. Glazov, T. F. Heinz, X. Marie, T. Amand, and B. Urbaszek, Colloquium: Excitons in atomically thin transition metal dichalcogenides, *Rev. Mod. Phys.* **90**, 021001 (2018).
- [4] A. Laturia, M. L. Van de Put, and W. G. Vandenberghe, Dielectric properties of hexagonal boron nitride and transition metal dichalcogenides: from monolayer to bulk, *npj 2D Mater. Appl.* **2**, 6 (2018).
- [5] Z. Zhou, Y. Zhang, and Z. Zhang, Optical and electrical properties of two-dimensional anisotropic crystals, *J. Semicond.* **40**, 061001 (2019).
- [6] A. Arora, Magneto-optics of layered two-dimensional semiconductors and heterostructures: Progress and prospects, *J. Appl. Phys.* **129**, 120902 (2021).
- [7] C. Meineke, J. Schlosser, M. Zizlsperger, M. Liebich, N. Nilforoushan, K. Mosina, S. Terres, A. Chernikov, Z. Sofer, M. A. Huber, M. Florian, M. Kira, F. Dirnberger, and R. Huber, Ultrafast exciton dynamics in the atomically thin van der waals magnet crsbr, *Nano Lett.* **24**, 4101 (2024).
- [8] Z. Lian, Y.-M. Li, L. Yan, L. Ma, D. Chen, T. Taniguchi, K. Watanabe, C. Zhang, and S.-F. Shi, Stark effects of Rydberg excitons in a monolayer WSe_2 P-N junction, *Nano Lett.* **24**, 4843 (2024).
- [9] H. Okamura, S. Iguchi, T. Sasaki, Y. Ikemoto, T. Moriwaki, and Y. Akahama, Interband spectroscopy of landau levels and magnetoexcitons in bulk black phosphorus, *Phys. Rev. B* **111**, 125202 (2025).
- [10] A. S. Rodin, A. Carvalho, and A. H. Castro Neto, Excitons in anisotropic two-dimensional systems, *Phys. Rev. B* **90**, 075429 (2014).
- [11] J. H. Choi, P. Cui, H. Lan, and Z. Zhang, Linear scaling of the exciton binding energy versus the band gap of two-dimensional materials, *Phys. Rev. Lett.* **115**, 066403 (2015).
- [12] H. M. Hill, A. F. Rigosi, C. Roquelet, A. Chernikov, T. C. Berkelbach, D. R. Reichman, M. S. Hybertsen, L. E. Brus, and T. F. Heinz, Observation of excitonic Rydberg states in monolayer MoS_2 and WS_2 by photoluminescence excitation spectroscopy, *Nano Lett.* **15**, 2992 (2015).
- [13] A. V. Stier, N. P. Wilson, K. A. Velizhanin, J. Kono, X. Xu, and S. A. Crooker, Magneto-optics of exciton Rydberg states in a monolayer semiconductor, *Phys. Rev. Lett.* **120**, 057405 (2018).
- [14] P. D.-A. Nguyen, D.-N. Ly, D.-N. Le, D. N.-T. Hoang, and V.-H. Le, High-accuracy energy spectra of a two-dimensional exciton screened by reduced dimensionality with the presence of a constant magnetic field, *Phys. E: Low-Dimens. Syst. Nanostructures* **113**, 152 (2019).
- [15] M. Goryca, J. Li, A. V. Stier, T. Taniguchi, K. Watanabe, E. Courtade, S. Shree, C. Robert, B. Urbaszek, X. Marie, and S. A. Crooker, Revealing exciton masses and dielectric properties of monolayer semiconductors with high magnetic fields, *Nat. Commun.* **10**, 4172 (2019).
- [16] W.-T. Hsu, J. Quan, C.-Y. Wang, L.-S. Lu, M. Campbell, W.-H. Chang, L.-J. Li, X. Li, and C.-K. Shih, Dielectric impact on exciton binding energy and quasiparticle bandgap in monolayer WS_2 and WSe_2 , *2D Mater.* **6**, 025028 (2019).
- [17] S.-Y. Chen, Z. Lu, T. Goldstein, J. Tong, A. Chaves, J. Kunstmann, L. S. R. Cavalcante, T. Woźniak, G. Seifert, D. R. Reichman, T. Taniguchi, K. Watanabe, D. Smirnov, and J. Yan, Luminescent emission of excited rydberg excitons from monolayer WSe_2 , *Nano Lett.* **19**, 2464 (2019).
- [18] E. Liu, J. van Baren, T. Taniguchi, K. Watanabe, Y.-C. Chang, and C. H. Lui, Magnetophotoluminescence of exciton Rydberg states in monolayer WSe_2 , *Phys. Rev. B* **99**, 205420 (2019).

- [19] D.-N. Ly, D.-N. Le, D.-A. P. Nguyen, N.-T. D. Hoang, N.-H. Phan, H.-M. L. Nguyen, and V.-H. Le, Retrieval of material properties of monolayer transition metal dichalcogenides from magnetoexciton energy spectra, *Phys. Rev. B* **107**, 205304 (2023).
- [20] S. Takahashi, S. Kusaba, K. Watanabe, T. Taniguchi, K. Yanagi, and K. Tanaka, 3D hydrogen-like screening effect on excitons in hBN-encapsulated monolayer transition metal dichalcogenides, *Sci. Rep.* **14**, 27286 (2024).
- [21] D.-N. Ly, D.-N. Le, D.-K. D. Le, and V.-H. Le, Retrieval of fundamental material parameters of monolayer transition metal dichalcogenides from experimental exciton energies: An analytical approach, *Phys. Rev. B* **112**, 165417 (2025).
- [22] F. Lu, Q. Hu, Y. Xu, and H. Yu, Coupled exciton internal and center-of-mass motions in two-dimensional semiconductors by a periodic electrostatic potential, *Phys. Rev. B* **109**, 165422 (2024).
- [23] F. Ferreira and R. M. Ribeiro, Improvements in the GW and Bethe-Salpeter-equation calculations on phosphorene, *Phys. Rev. B* **96**, 115431 (2017).
- [24] P. E. Faria Junior, M. Kurpas, M. Gmitra, and J. Fabian, k-p theory for phosphorene: Effective g-factors, Landau levels, and excitons, *Phys. Rev. B* **100**, 115203 (2019).
- [25] J. Li, J. Ma, X. Cheng, Z. Liu, Y. Chen, and D. Li, Anisotropy of excitons in two-dimensional perovskite crystals, *ACS Nano* **14**, 2156 (2020).
- [26] S. H. Suk, S. B. Seo, Y. S. Cho, J. Wang, and S. Sim, Ultrafast optical properties and applications of anisotropic 2d materials, *Nanophotonics* **13**, 107 (2024).
- [27] D. T.-X. Dang, D.-N. Le, and L. M. Woods, Twisting in h-bn bilayers and their angle-dependent properties, *Phys. Rev. B* **112**, 085102 (2025).
- [28] L. Vannucci, U. Petralanda, A. Rasmussen, T. Olsen, and K. S. Thygesen, Anisotropic properties of monolayer 2D materials: An overview from the C2DB database, *J. Appl. Phys.* **128**, 105101 (2020).
- [29] M. N. Gjerding, A. Taghizadeh, A. Rasmussen, S. Ali, F. Bertoldo, T. Deilmann, N. R. Knøsgaard, M. Kruse, A. H. Larsen, S. Manti, T. G. Pedersen, U. Petralanda, T. Skovhus, M. K. Svendsen, J. J. Mortensen, T. Olsen, and K. S. Thygesen, Recent progress of the computational 2d materials database (c2db), *2D Mater.* **8**, 044002 (2021).
- [30] V. Tran, R. Soklaski, Y. Liang, and L. Yang, Layer-controlled band gap and anisotropic excitons in few-layer black phosphorus, *Phys. Rev. B* **89**, 235319 (2014).
- [31] A. Chaves, T. Low, P. Avouris, D. Çakır, and F. M. Peeters, Anisotropic exciton Stark shift in black phosphorus, *Phys. Rev. B* **91**, 155311 (2015).
- [32] A. M. Wang, K. L. Seyler, V. Tran, Y. Jia, H. Zhao, H. Wang, L. Yang, X. Xu, and F. Xia, Highly anisotropic and robust excitons in monolayer black phosphorus, *Nat. Nanotechnol.* **10**, 517 (2015).
- [33] J. O. Island, G. A. Steele, H. S. J. van der Zant, and A. Castellanos-Gomez, Titanium trisulfide (TiS₃): a 2D semiconductor with quasi-one-dimensional properties, *Sci. Rep.* **6**, 22214 (2016).
- [34] C. E. Villegas, A. S. Rodin, A. Carvalho, and A. R. Rocha, Two-dimensional exciton properties in monolayer semiconducting phosphorus allotropes, *Phys. Chem. Chem. Phys.* **18**, 27829 (2016).
- [35] C. J. Paez, K. DeLello, D. Le, A. L. C. Pereira, and E. R. Mucciolo, Disorder effect on the anisotropic resistivity of phosphorene determined by a tight-binding model, *Phys. Rev. B* **94**, 165419 (2016).
- [36] E. Torun, H. Sahin, A. Chaves, L. Wirtz, and F. M. Peeters, Ab initio and semiempirical modeling of excitons and trions in monolayer tis₃, *Phys. Rev. B* **98**, 075419 (2018).
- [37] M. Van der Donck and F. M. Peeters, Excitonic complexes in anisotropic atomically thin two-dimensional materials: Black phosphorus and TiS₃, *Phys. Rev. B* **98**, 235401 (2018).
- [38] G. Zhang, A. Chaves, S. Huang, F. Wang, Q. Xing, T. Low, and H. Yan, Determination of layer-dependent exciton binding energies in few-layer black phosphorus, *Sci. Adv.* **4**, eaap9977 (2018).
- [39] J. C. G. Henriques and N. M. R. Peres, Excitons in phosphorene: A semi-analytical perturbative approach, *Phys. Rev. B* **101**, 035406 (2020).
- [40] F. Wang, C. Wang, A. Chaves, C. Song, G. Zhang, S. Huang, Y. Lei, Q. Xing, L. Mu, Y. Xie, and H. Yan, Prediction of hyperbolic exciton-polaritons in monolayer black phosphorus, *Nat. Comm.* **12**, 5628 (2021).
- [41] S. Wu, Anisotropic exciton states and excitonic absorption spectra in a freestanding monolayer black phosphorus, *Phys. E: Low-Dimens. Syst. Nanostructures.* **141**, 115238 (2022).
- [42] R. Y. Kezerashvili, M. R. Haywood, and D. L. Boykin, Magnetoexcitons in phosphorene monolayers, bilayers, and heterostructures, *Phys. Rev. Research* **4**, 013154 (2022).
- [43] R. Y. Kezerashvili and A. Spiridonova, Anisotropic magnetoexcitons in two-dimensional transition metal trichalcogenide semiconductors, *Phys. Rev. Res.* **4**, 033016 (2022).
- [44] L. Li, Y. Yu, G. J. Ye, Q. Ge, X. Ou, H. Wu, D. Feng, X. H. Chen, and Y. Zhang, Black phosphorus field-effect transistors, *Nat. Nanotechnol.* **9**, 372 (2014).
- [45] A. Avsar, I. J. Vera-Marun, J. Y. Tan, K. Watanabe, T. Taniguchi, A. H. Castro Neto, and B. Özyilmaz, Air-stable transport in graphene-contacted, fully encapsulated ultrathin black phosphorus-based field-effect transistors, *ACS Nano* **9**, 4138 (2015).
- [46] S. Das, A. Sebastian, E. Pop, C. J. McClellan, A. D. Franklin, T. Grasser, T. Knobloch, Y. Illarionov, A. V. Penumatcha, J. Appenzeller, Z. Chen, W. Zhu, I. Asselberghs, L.-J. Li, U. E. Avci, N. Bhat, T. D. Anthopoulos, and R. Singh, Transistors based on two-dimensional materials for future integrated circuits, *Nat. Electron.* **4**, 786–799 (2021).
- [47] Y. Liu, X. Duan, H.-J. Shin, S. Park, Y. Huang, and X. Duan, Promises and prospects of two-dimensional transistors, *Nature* **591**, 43–53 (2021).
- [48] X. Huang, C. Liu, and P. Zhou, 2D semiconductors for specific electronic applications: from device to system, *npj 2D Mater. Appl.* **6**, 51 (2022).
- [49] N. S. Rytova, Screened potential of a point charge in a thin film, *Moscow University Physics Bulletin* **22**, 30 (1967).
- [50] L. V. Keldysh, Coulomb interaction in thin semiconductor and semimetal films, *JETP Lett.* **29**, 658 (1979).
- [51] J. E. Avron, I. W. Herbst, and B. Simon, Separation of center of mass in homogeneous magnetic fields, *Ann. Phys.* **114**, 431 (1978).
- [52] B. R. Johnson, J. O. Hirschfelder, and K.-H. Yang, Interaction of atoms, molecules, and ions with constant

- electric and magnetic fields, *Rev. Mod. Phys.* **55**, 109 (1983).
- [53] H. Ruder, G. Wunner, H. Herold, and F. Geyer, *Atoms in Strong Magnetic Fields* (Springer - Verlag, Berlin, 1994).
- [54] L. V. Butov, C. W. Lai, D. S. Chemla, Y. E. Lozovik, K. L. Campman, and A. C. Gossard, Observation of magnetically induced effective-mass enhancement of quasi-2d excitons, *Phys. Rev. Lett.* **87**, 216804 (2001).
- [55] D.-N. Ly, D.-N. Le, N.-H. Phan, and V.-H. Le, Thermal effect on magnetoexciton energy spectra in monolayer transition metal dichalcogenides, *Phys. Rev. B* **107**, 155410 (2023).
- [56] L. D. Landau and E. M. Lifshitz, *Quantum Mechanics: Non-relativistic Theory* (Pergamon, Oxford, 1977).
- [57] A. Galiautdinov, Anisotropic keldysh interaction, *Phys. Lett. A* **383**, 3167 (2019).
- [58] I. D. Feranchuk and L. I. Komarov, The operator method of the approximate solution of the Schrödinger equation, *Phys. Lett. A* **88**, 211 (1982).
- [59] I. Feranchuk, A. Ivanov, V. H. Le, and A. Ulyanenko, *Non-perturbative Description of Quantum Systems*, Springer Tracts in Modern Physics, Vol. 894 (Springer International Publishing, Cham, 2015).
- [60] L. V. Hoang and N. T. Giang, The algebraic method for two-dimensional quantum atomic systems, *J. Phys. A: Math. Gen.* **26**, 1409 (1993).
- [61] Netlib.org. LAPACK: Linear Algebra PACKage, [Subroutine dsygvx.f](http://netlib.org/dsygvx.f).